Available online at www.sciencedirect.com
SCIENCE DIRECT®
Journal of Molecular Structure 655 (2003) 269–277
Journal of MOLECULAR STRUCTURE
www.elsevier.com/locate/molstruc

Quinoprotein methanol dehydrogenase: a molecular dynamics study and comparison with crystal structure

Swarnalatha Y. Reddy[a,*], F. Scott Mathews[b], Ya-Jun Zheng[c], Thomas C. Bruice[a]

[a]*Department of Chemistry and Biochemistry, University of California, Santa Barbara, CA 93106, USA*
[b]*Department of Biochemistry and Molecular Biophysics, Washington University School of Medicine, St. Louis, MO 63110, USA*
[c]*DuPont Agricultural Products, Stine–Haskell Research Center, Newark, DE 19714, USA*

Received 6 February 2003; revised 12 April 2003; accepted 16 April 2003

Abstract

One of the mechanisms proposed for methanol oxidation by methanol dehydrogenase (MDH) involves a hydride transfer to the quinone carbonyl carbon C5 of 2,7,9-tricarboxy-1H-pyrrolo[2,3-f]-quinoline-4,5-dione (PQQ), initiated by abstraction of a proton from the substrate methanol by a general base. Molecular dynamics studies are performed on MDH-bound to the C5 reduced intermediate (C5RI) of PQQ, for 3 ns. The structural features of the MD and X-ray structures are compared. An interesting feature observed during simulations is the strong hydrogen bond between oxyanion O5 of C5RI and Asp297–CO_2H in the active site. Asp297–CO_2^- is suggested to be the general-base catalyst for removing the hydroxyl proton of methanol in concert with the hydride ion transfer from the putative methoxide to C5 carbonyl of PQQ. The formed Asp297–CO_2H acts as the required proton source for the immediate product. Anticorreleated motions observed in the MD structure are not across the active site to influence the reaction mechanism of MDH.

Keywords: Quinoprotein; Methanol dehydrogenase; 2,7,9-Tricarboxy-1H-pyrrolo[2,3-f]-quinoline-4,5-dione; Molecular dynamics

1. Introduction

Methanol dehydrogenase (MDH), a quino protein requires PQQ (2,7,9-tricarboxy-1H-pyrrolo[2,3-f]-quinoline-4,5-dione) [1–5] and a divalent cation Ca^{2+}, for catalytic activity [6–8]. Of the two mechanisms proposed for methanol oxidation by MDH, one involves a general base-catalyzed proton abstraction from methanol in concert with hydride transfer from the putative methoxide to the quinone carbonyl carbon, C5, and subsequent tautomerization to the hydroquinone $PQQH_2$ (Fig. 1) [9–12]. The other mechanism involves the nucleophilic addition of the putative methoxide to the carbonyl C5 of PQQ to form a hemiketal intermediate, followed by an intramolecular retro-ene reaction [9,13–17].

The crystal structures from methylotrophic bacteria, *Methylophilus* W3A1 [12,17,18] and *Methylobacterium extorquens* AM1 [19] have revealed that the MDH is a heterotetramer of two heavy and two light subunits, with a net molecular weight of 140 kDa. The elongated chains of the light subunits

* Corresponding author. Tel.: +1-805-893-2044; fax: + 1-805-893-2229..
E-mail address: tcbruice@bioorganic.ucsb.edu (T.C. Bruice).

0022-2860/03/$ - see front matter © 2003 Elsevier Science B.V. All rights reserved.
doi:10.1016/S0022-2860(03)00257-6

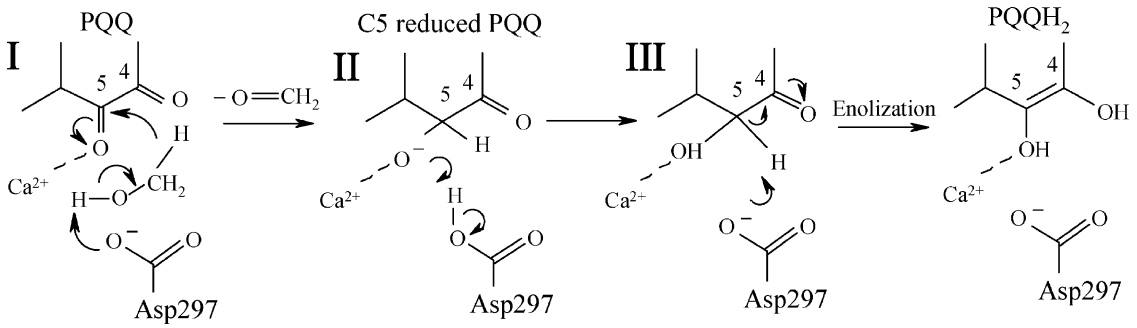

Fig. 1. Hydride transfer mechanism for methanol oxidation by MDH involving the C5 reduced intermediate of PQQ.

(8 kDa), extend over the surface of the heavy subunit (62 kDa), and apparently have no direct functional role in the redox reactions. Performance of molecular dynamics (MD) simulations of structures provided by X-ray crystallographic study is a useful endeavor, if one is interested in enzyme structural motions in aqueous solution. Besides, MD allows an extensive sampling of the phase space on real time scale. Here, we report MD studies of the MDH-bound to C5 reduced intermediate of PQQ (C5RI) complex (**II** of Fig. 1) in water for a period of 3 nano seconds (ns). A direct comparison of MD and X-ray structures are likely to enhance the understanding of structural variations. A particular interest is the positioning of the active site residue Asp297, which has been proposed as a proton donor in the hydride transfer mechanism of methanol oxidation by MDH [9,12,17].

2. Method

To obtain the partial atomic charges, the cofactor C5RI in the presence of Ca^{2+} was optimized at the HF/6-31 + G(d,p) level using GAUSSIAN 98 [20]. The electrostatic potential was calculated at the MP2/6-31 + G(d,p) level using the Merz–Singh–Kollman scheme [21]. The restrained electrostatic potential (RESP) method [22] was used to fit the electrostatic potential using an atom-centered point charge model. The starting structure (1.9 Å resolution) of C5RI containing the MDH hetrotetramer with 571 and 57 residues in each heavy (A and C) and light (B and D) subunits, respectively, was taken from the entry 1G72 of the Protein Data Bank [12]. The structure with 614 crystal waters was minimized for 500 steps of steepest descent (SD) and 1500 steps of adopted basis Newton–Raphson (ABNR) methods using the program CHARMM [23] (version c27b4) and CHARMM27 all-atom force field parameters [24]. The system was solvated in an equilibrated TIP3P [25] water sphere of 42 Å radius using the center of mass of the C5RI bound to subunit A as the origin. Any solvent molecule within 2.8 Å of heavy atoms was deleted. The MDH·C5RI complex contains a total of 36,694 atoms. As per **II** of Fig. 1, one of the carboxylate oxygens (OD1) of Asp297 was protonated for simulation. Positions of water molecules were minimized for 200 steps of SD followed by 2000 steps of ABNR methods, keeping the enzyme complex fixed. After that, the entire system was minimized for 2000 steps by the ABNR method before starting simulations.

Stochastic boundary molecular dynamics (SBMD) [26] was carried out using the program CHARMM. For SBMD, 40 Å reaction zone with a 2 Å buffer region (between 41 and 42 Å) from cofactor of subunit A was used. All the enzyme atoms that were at a distance beyond 42 Å from the center of mass were constrained after the minimization. An integration time step of 1.5 femto seconds (fs) and a constant dielectric of unity were used. Lennard–Jones interactions were truncated at a distance of 12 Å. SHAKE was applied to all covalent bonds involving hydrogens [27].

As the active sites in both heavy subunits of MDH are identical, the analysis was restricted to the trajectories of subunit A. The root-mean-square deviation (RMSD) values were evaluated by least-squares fitting the backbone heavy atoms of the enzyme to the minimized structure. Based on the stabilization of the RMSD values, MD structure

was averaged during the period 2.116–3.00 ns for analysis. The positional fluctuations of C_α in the protein backbone were calculated from the MD trajectory, by least-squares fitting of all the atoms of the complex at 0.75 pico seconds intervals, averaged over the period from 2.116 to 3.00 ns. The crystal structure positional fluctuations were evaluated using the equation $(\Delta r^2)^{1/2} = (3B/8\pi^2)^{1/2}$ from experimental Debye–Waller B-factors. Cross correlation between atomic fluctuations were estimated by calculating the covariance between fluctuations of two residues, averaged by residue over C_α atoms of enzyme in each structure.

3. Results and discussion

3.1. Mean square deviations and positional fluctuations

The RMSD values of the backbone heavy atoms of the MDH·C5RI complex with respect to the minimized X-ray structure for 3 ns are given in Fig. 2(a). The plot indicates the gradual increase in values, with a maximum value of 1.5 Å, and stabilizes during the period 2–3 ns. Atomic fluctuations of C_α atoms of the enzyme for the MDH·C5RI complex are shown in Fig. 2(b). The majority of the positional fluctuations estimated from the B-factors of the crystal structure (solid line) are greater than the values calculated from the MD simulated structures. This may be due either to the mosaicity of the crystal or the inadequate conformational sampling during dynamics. A few sharp peaks are observed in the regions of residues 309–316, 370–374 and 450–457 of the MD structure. These values are higher than those from the X-ray data and correspond to interstrand loops. Overall, MD simulations reproduce the trends in fluctuations of the enzyme.

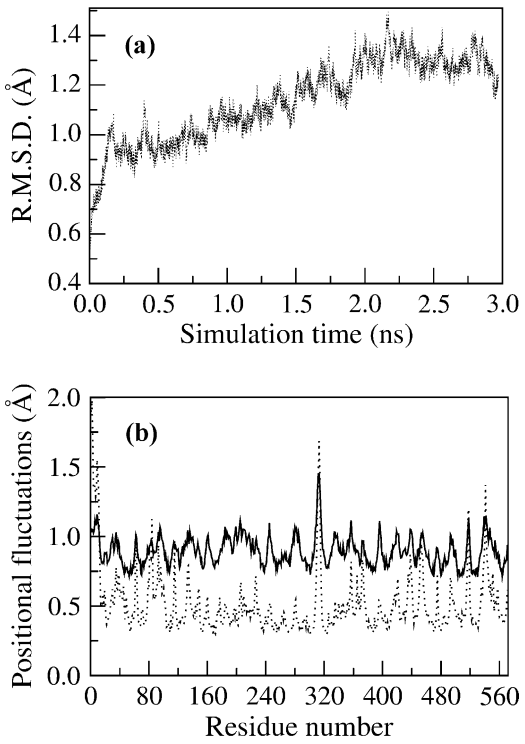

Fig. 2. (a) Root mean-square deviations (RMSD) of the backbone heavy atoms of the A subunit of the C5RI complex relative to the minimized structure during dynamics; (b) atomic fluctuations of C_α atom of the protein backbone of subunit A of the MD averaged MDH·C5RI (dotted line) complex compared to the crystal structure (solid line).

3.2. Coordination of calcium ion

Ca^{2+} is likely to stabilize the electrophilic C5 of cofactor for attack by the hydride. In the MDH crystal structure Ca^{2+} is hexacoordinated with three of its six ligands supplied by cofactor. These are the C7 carboxylate oxygen, O7A, pyridine nitrogen N6 and C5 oxygen, O5 of C5RI. The other three ligands to Ca^{2+} are the side chain oxygens of Glu171 and Asn255. A comparison of Ca^{2+} coordination distances between the X-ray and MD structures, shown in Fig. 3, indicates the separations are shorter in the MD structure. During the MD simulation Ca^{2+} retains hexacoordination, and the distances to N6, O7A and O5 of C5RI are 2.20, 2.43 and 2.07 Å, respectively. The average bonding distances from Ca^{2+} to the carboxylate oxygens (OE1 and OE2) of Glu171, and the amide oxygen (OD1) of Asn255 of the enzyme are approximately the same (Fig. 3).

3.3. Amino acids and crystal waters of the active site

Each heavy subunit (62 kDa) of MDH is associated with a calcium ion and one PQQ molecule non-covalently bound in the active site. Based on the separation between Ca^{2+} and O5 oxygen of

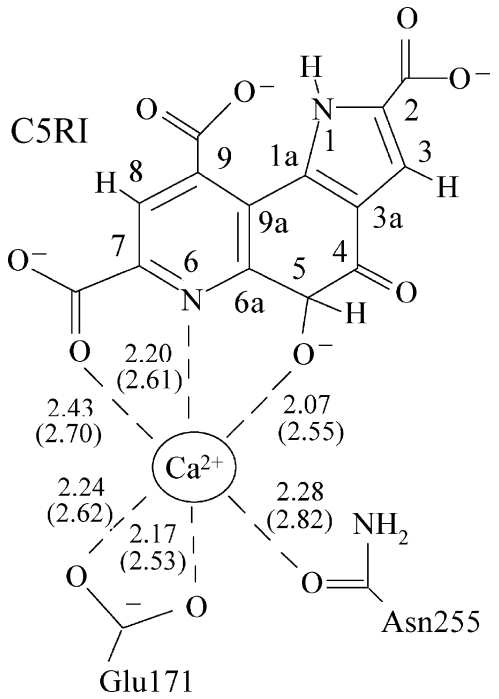

Fig. 3. Chemical structure of C5RI and coordination of Ca^{2+} in the active site of MDH. Distances to Ca^{2+} in the MD averaged and X-ray (in bracket) structures are given in Å.

cofactor (2.55 Å) in the subunit A of the X-ray data [12], the C5RI structure most likely corresponds to that with oxyanion, rather than protonated oxygen at O5 (Fig. 1). This is because the distance $O^{-}\cdots Ca^{2+}$ is estimated to be shorter than $H{-}O\cdots Ca^{2+}$. A superimposed stereo plot of a few residues of the active site of the MD averaged and X-ray structures of the MDH·C5RI complex are shown in Fig. 4. An inversion of O5 atom at tetrahedral C5, pointing towards Glu171 in the MD structure is observed. Other significant movements noticed between the MD and X-ray structures are: Wat1 by a few 10ths of an Å, Asp297 towards O5 oxygen of C5RI and Asn387 away from C4 carbonyl oxygen O4 of C5RI by nearly 1 Å.

3.4. Role of Asp297

A comparison of conformational features and the interactions in the active site between the MD averaged and X-ray structures are given in Fig. 5. Asp297–CO_2H has been proposed to act as a proton donor to the O5 oxygen of intermediate **II** of Fig. 1 [9,12,17]. A time variation plot of the separation of O5 oxygen of C5RI and the protonated carboxylate oxygen (OD1) of Asp297 is provided in Fig. 6. Distinctly, after 60 ps of dynamics Asp297–CO_2H has moved close enough to form a stable hydrogen bond with oxyanion O5 (2.57 ± 0.08 Å). This is an interesting feature observed in the MD simulation, as the corresponding separation in the crystal structure is 4.07 Å.

3.5. Motions of crystal waters

As observed earlier in the crystal structure, seven waters proximal to the cofactor are present during MD simulation. These are shown in stereo plot of the MD averaged structure of the MDH·C5RI complex (Fig. 7). The crystal water Wat1 forms hydrogen bonds with O5 oxygen and tetrahedral C5–H5 of

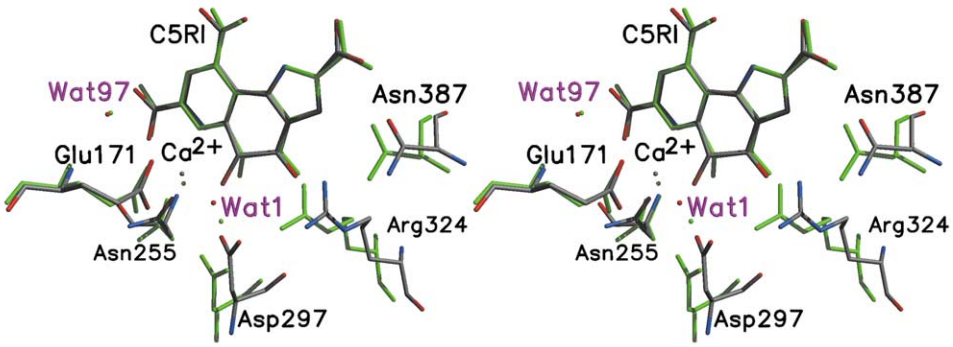

Fig. 4. Stereoview of superposition of the active site residues of MD averaged and X-ray structures of the MDH·C5RI complex. The X-ray structure is shown in green. Hydrogens of the MD structure are not shown.

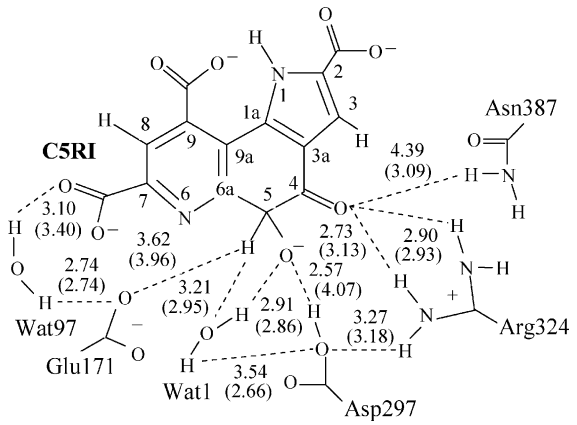

Fig. 5. Essential residues in the active site of MDH·C5RI complex. Numerical values of distances (Å) between heavy atoms are given for the MD averaged and X-ray (in bracket) structures.

C5RI (Fig. 5) in both the MD and X-ray structures. The separation of Wat1 and the carboxylate oxygen (OD1) of Asp297 in the X-ray structure is 2.66 Å, while in the MD structure the value fluctuates, with an average value 3.54 ± 0.36 Å. Wat1 is positioned 3.58 ± 0.19 Å from CZ2 zeta carbon of Trp259 and 3.73 ± 0.44 Å from CH2 ring carbon atom of Trp531 in the MD structure, while separations are ~0.4 Å smaller (3.21 and 3.31 Å, respectively) in the crystal structure.

Five of the other crystal waters, Wat63 to Wat66 and Wat97 form a cluster (upper left of Fig. 7) in both the MD and X-ray structures. One of these, Wat65, forms a hydrogen bond (2.86 Å) with the C9 carboxylate oxygen, O9B of the cofactor in the crystal structure, while the separation is large

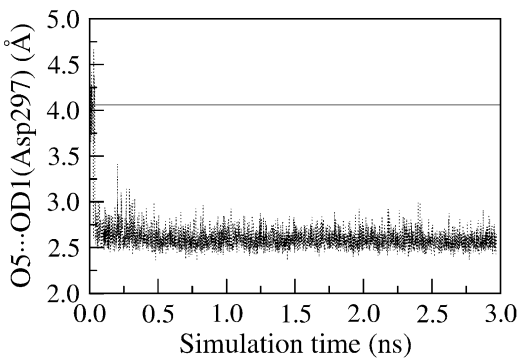

Fig. 6. Time dependent variation of distance between the protonated carboxylate oxygen of Asp297–OD1 and anionic O5 of C5RI in the MD complex. The X-ray structure value is shown as the solid line.

(3.82 ± 0.57 Å) during dynamics. Wat97 forms a hydrogen bond with the carboxylate oxygen (OE1) of Glu171 (Fig. 5) consistent with the crystal structure. Wat91, away from the other water molecules, forms hydrogen bonds with the C7 carboxylate oxygen, O7A (Fig. 7), indole nitrogen of Trp237, hydroxyl oxygen of Thr235, amide oxygen and backbone nitrogen of Asn255 in both the X-ray and MD structures (Table 1).

3.6. Interactions with Arg324

Interaction of Arg324, as well as Ca^{2+} with the oxygen at the tetrahedral C5 would be expected to assist hydride or nucleophilic addition to the C5 carbonyl of PQQ. In the X-ray structure the separation between guanido nitrogen NH1 of Arg324 and oxyanion O5 of C5RI is 3.03 Å, while NH1 and O5 drift away from each other during the simulation. In place, O5 oxygen is hydrogen bonded, to Asp297–CO_2H in the MD structure, and also with Wat1 (Fig. 5). The proton (HH11) on guanido NH1 of Arg324 engages in favorable interactions with the carboxylate oxygen (OD1) of Asp297, while the proton HH12 at NH1 of Arg324 with the carbonyl oxygen of Asp297 during simulation. These interactions are in good agreement with the crystal structure. The C4 carbonyl oxygen, O4 of C5RI hydrogen bonds to NH1–HH11 and NH2–HH22 of Arg324 in both the MD and X-ray structures, though the separations are slightly higher in the latter.

3.7. Other interactions of C5RI

Besides the aforementioned interactions of C5RI with Asp297, Arg324 and crystal waters, there is a network of hydrogen bond interactions and salt bridges that involve 2, 7 and 9 carboxylate oxygens of cofactor (Fig. 7). As seen in Table 1, most of the non-bonded separations related to these interactions of the MD complex are consistent with the crystal structure [12]. An observed distinct difference is that, the C4 carbonyl oxygen, O4 of C5RI hydrogen bonds to amide side chain of Asn387 (3.09 Å) in the X-ray structure, while the value of this distance is markedly greater (4.39 ± 0.33 Å) during simulation, indicating a lack of hydrogen bonding (Fig. 5).

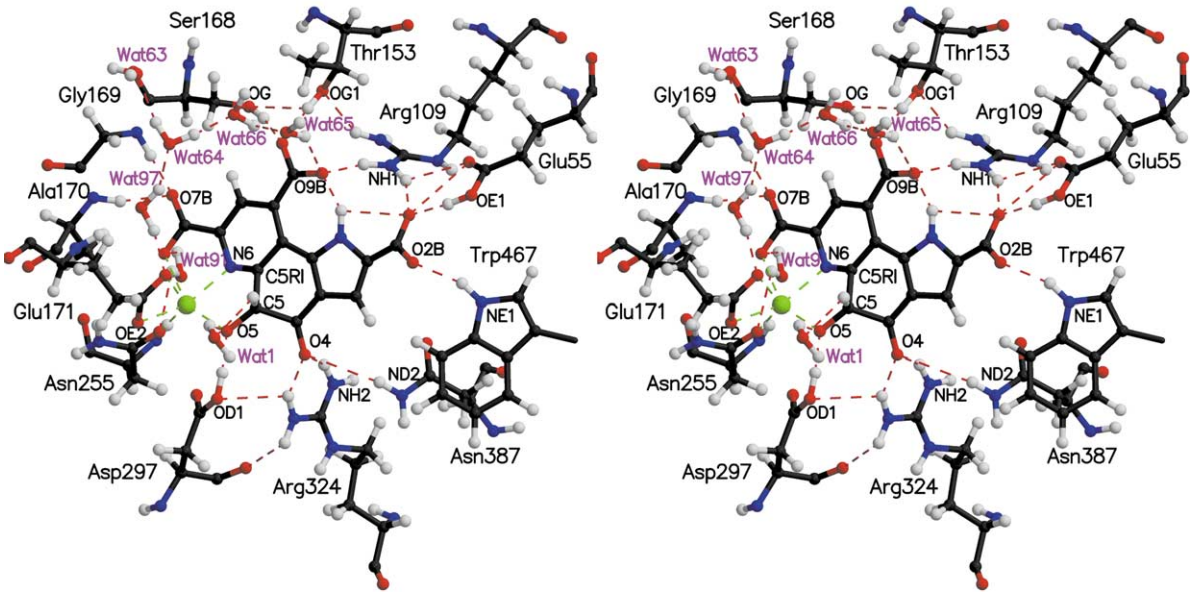

Fig. 7. Stereoplot of the active site depicting equatorial interactions of the MD averaged MDH·C5RI complex. Non-bonded interactions are shown by red dashed lines and Ca^{2+} coordination is in green.

3.8. Conformation of disulphide ring

The vicinal disulphide Cys103–Cys104 near the cofactor is a novel feature of MDH. The reduction of the disulphide bond has been shown to result in loss of enzyme activity [28]. The average value of the peptide bond torsion angle of the vicinal disulphide favors a *trans* configuration (212°) in the MD averaged structure. The strain due to the unusual *trans* configuration of the peptide bond is compensated by deviations of torsion angles, χ of Cys103, ϕ and ψ of Asp105, from the generally preferred values. The torsion angles χ of Cys103 are 68° and ϕ and ψ of Asp105 are 69 and 171°, respectively. Overall, these features are similar to those observed in the X-ray structure.

3.9. Configuration of the C5RI ring

The proximity of Ca^{2+} to O5 oxygen might stabilize the O5 oxyanion and the tetrahedral geometry of the C5 carbon. The average bond angles related to ∠C5 (C6a–C5–C4, C6a–C5–O5, C4–C5–O4) and ∠C4 (C3a–C4–C5, C3a–C4–O4, C5–C4–O4) centers of cofactor are 115 and 119°,

Table 1
Non-bonded distances (Å) between various atoms in the active site and their standard deviations (in parentheses) of the MD averaged (2.116–3.00 ns) and X-ray structures of MDH·C5RI complex

Non-bonded distances	X-ray	MD average
O7A···O (Wat91)	2.86	2.74 (±0.14)*
OG1 (Thr235)···O (Wat91)	2.97	2.82 (±0.14)*
NE1 (Trp237)···O (Wat91)	2.91	3.36 (±0.35)**
N (Asn255)···O (Wat91)	3.32	2.94 (±0.13)**
OD1 (Asn255)···O (Wat91)	2.87	2.99 (±0.16)*
O9B···O (Wat65)	2.89	3.82 (±0.57)
N1···O9B	2.54	2.55 (±0.05)*
N1···O2A	2.86	2.76 (±0.07)*
O2A···NH1 (Arg109)	2.97	2.85 (±0.16)*
O2A···OE1 (Glu55)	2.48	2.71 (±0.11)*
O2A···OE2 (Glu55)	3.15	3.22 (±0.18)*
O2B···NE1 (Trp467)	2.86	3.11 (±0.30)*
O2B···N (Trp531)	3.04	2.89 (±0.15)*
O7B···OG1 (Thr235)	2.79	2.80 (±0.16)*
O7B···N (Gly169)	2.73	2.76 (±0.10)*
O7B···N (Ala170)	3.15	2.98 (±0.15)*
O9A···OG (Ser168)	2.85	2.77 (±0.20)*
O9A···OG1 (Thr153)	2.55	2.67 (±0.10)*
O9B···NH1 (Arg109)	3.04	2.66 (±0.09)**
OG (Ser168)···OG1 (Thr153)	3.18	3.12 (±0.18)*
OG1 (Thr153)···NH2 (Arg109)	2.83	2.97 (±0.17)*
OE2 (Glu55)···NH1 (Arg109)	3.55	3.15 (±0.19)**

Values within *0.25 and **0.26–0.45 Å different than the crystal structure.

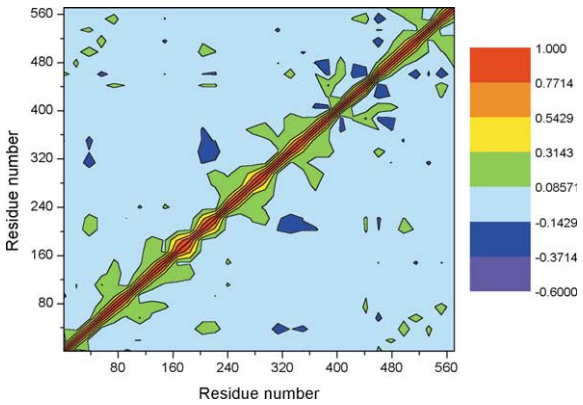

Fig. 8. Cross correlation of residue–residue fluctuations of C_α atom of the MD averaged MDH·C5RI complex. The range of correlations is indicated by the various colors of the panel.

respectively, while those of crystal structure are 120 and 107°, respectively. The C5 atom is, as expected out of plane compared to C4 carbonyl carbon of C5RI. This is indicated by the torsion angle, C3–C3A–C4–C5 preferring a value of 157° in the MD structure compared to the X-ray value 164°, while the torsion angle N1–C1A–C3A–C4 favors a value 182° in both structures.

3.10. Atomic motions of the MD structure

Analyses of the correlated and anticorrelated atomic motions reveal the influence of motions directed at great distances from the active site. Cross-correlations of residue–residue motions of C_α atoms of the MD averaged MDH·C5RI complex are given in Fig. 8. Anti-correlated motions (dark blue) are observed among the residues: (i) 305–355 with 35–45, (ii) 305–365 with 180–225, (iii) 445–475 with 370–380, and 420–440, (iv) 505–515, and 540–555 with 455–465. Significantly, the active site residue Arg324 is involved in some of these motions. The positive correlated motions among a few residues are scattered (Fig. 8). The magnitude of these motions (green) is insignificant and henceforth not discussed.

The anticorrelated motions related to the secondary structural features of MDH are shown in Fig. 9. Each heavy subunit of MDH has a β-propeller fold composed of eight four-stranded antiparallel β-sheets, giving rise to an eight-fold axis of pseudosymmetry. The cofactor, C5RI is buried in a chamber close to the central channel of the β-propeller. The vicinal disulphide Cys103–Cys104 is colored yellow in

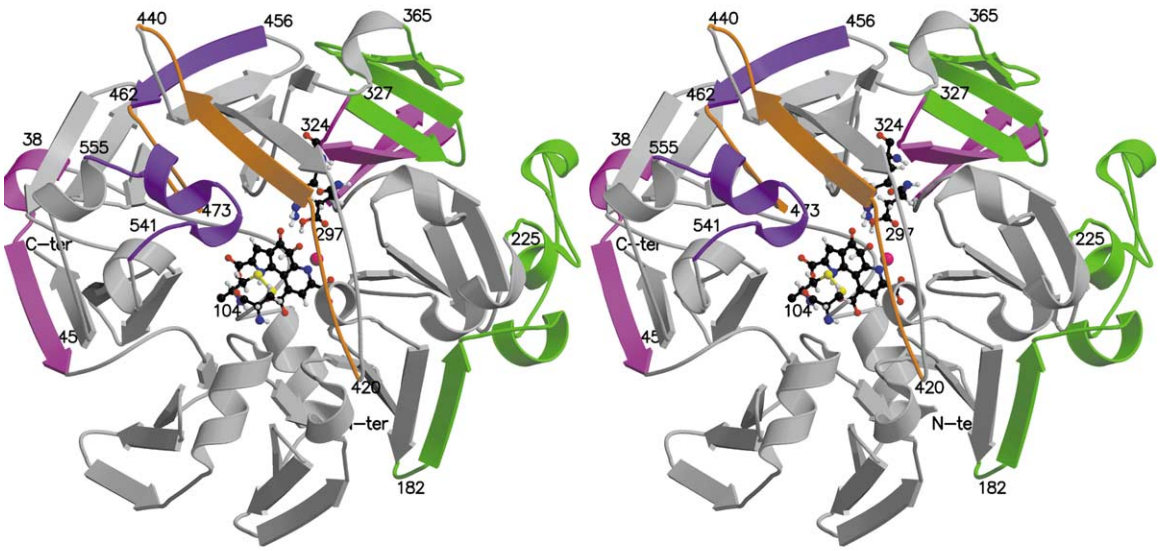

Fig. 9. Mapping of the anticorrelated motions in subunit A of the MD averaged MDH·C5RI structure. Ball and stick representation is used for the active site residues Asp297, Arg324, Cys103, Cys104 and also C5RI. Ca^{2+} is shown in pink. Notice C5RI is deep inside the pseudo eight-fold axis of the β-propeller. The negative correlated motions among residues are represented by the same color. Folding of other residues is displayed in gray.

Fig. 9. The residues that show anticorrelated motions are shown by the same color representation. Thus, anticorrelations among residues 305–355 with 36–47 are magenta, 327–365 with 182–225 are green, 462–475 with 420–440 are mustard and 456–462 with 540–555 are purple. For the sake of clarity multiple anticorrelations seen in Fig. 8, are not shown in Fig. 9. For instance, the coil and β-sheets in the residue range 305–355, where Arg324 resides, anticorrelates not only with residues 35–45 (magenta), but also with the stretch of residues 180–225 (green) (Fig. 9). Anticorrelated motions so observed are not diagonally through the active site. This indicates transmission of motions to distant parts of the enzyme would not influence reaction trajectories.

4. Conclusions

MD studies have been performed for 3 ns on the MDH-bound C5 reduced PQQ intermediate of the hydride transfer mechanism of methanol oxidation (**II** of Fig. 1). Hexacoordination of Ca^{2+}, observed in the X-ray structure is maintained during simulation of the MDH·C5RI complex. A strong hydrogen bond between the oxyanion, O5 of C5RI and crystal water, Wat1 during the entire dynamics (Fig. 5) is in good agreement with the X-ray structural studies [12,17].

Asp297–CO_2^- has been suggested [9,12,17,18] to be a general-base catalyst for removing the hydroxyl proton of methanol in concert with hydride ion transfer for the putative methoxide to the C5 carbonyl of PQQ (**I** of Fig. 1). In the second step of the reaction, the formed Asp297–CO_2H gives up its proton to the immediate product. This is not obvious in the crystal structure due to large separations between the carboxylate oxygens of Asp297 and the O5 of cofactor. During MD simulation, a strong hydrogen bond between the O5 oxygen of C5RI and Asp297–CO_2H is observed (Figs. 5 and 7). This supports Asp297–CO_2H as the required proton source for the immediate product (**II** of Fig. 1). A similar MD strategy adopted in the study of yeast chorismate mutase have shown that the protonated Glu246 leads to a stable structure [29]. Thus MD studies are valuable in revealing conformations that escape detection by X-ray crystallography.

The C4 carbonyl oxygen O4 of C5RI forms hydrogen bonds with the guanido, NH1 and NH2 of Arg324, consistent to the crystal structure [12]. These interactions are expected to assist rearrangement of the C5RI to the hydroquinone $PQQH_2$. Significant anticorrelated motions observed in the MD structure are too distant from the active site to affect the kinetics of enzyme.

Acknowledgements

Thanks to Devleena Mazumder for help. This work was supported by funds from the NIH (5R37DK0917136). We acknowledge computer time on UCSB's SGI Origin 2000 and at NPACI (San Diego Supercomputer Center).

References

[1] C. Anthony, L.J. Zatman, Biochem. J. 104 (1967) 960.
[2] T.S. Eckert, T.C. Bruice, J.A. Gainor, S.M. Weinreb, Proc. Natl Acad. Sci. USA 79 (1982) 2533.
[3] T.S. Eckert, T.C. Bruice, J. Am. Chem. Soc. 105 (1983) 4431.
[4] E.J. Rodriguez, T.C. Bruice, J. Am. Chem. Soc. 111 (1989) 7947.
[5] J.A. Duine, Eur. J. Biochem. 200 (1991) 271.
[6] O. Adachi, K. Matsushita, E. Shinagawa, M. Ameyama, Agric. Biol. Chem. 54 (1990) 2833.
[7] I.W. Richardson, C. Anthony, Biochem. J. 287 (1992) 709.
[8] S. White, G. Boyd, F.S. Mathews, Z. Xia, W.W. Dai, Y.F. Zhang, V.L. Davidson, Biochemistry 32 (1993) 12955.
[9] C. Anthony, Biochem. J. 320 (1996) 697.
[10] Y.-J. Zheng, T.C. Bruice, Proc. Natl Acad. Sci. USA 94 (1997) 11881.
[11] P.R. Afolabi, F. Mohammed, K. Amaratunga, O. Majekodunmi, S.L. Dales, R. Gill, D. Thompson, J.B. Cooper, S.P. Wood, P.M. Goodwin, C. Anthony, Biochemistry 40 (2001) 9799.
[12] Y.-J. Zheng, Z. Xia, Z. Chen, F.S. Mathews, T.C. Bruice, Proc. Natl Acad. Sci. USA 98 (2001) 432.
[13] R.H. Dekker, J.A. Duine, J. Frank, J.P. Eugene, J. Verwiel, J. Westerling, Eur. J. Biochem. 125 (1982) 69.
[14] J.J. Frank, S. Vankrimpen, P.E. Verwiel, J.A. Jongejan, A.C. Mulder, J.A. Duine, Eur. J. Biochem. 184 (1989) 187.
[15] S. Itoh, M. Ogino, Y. Fukui, H. Murao, M. Komatsu, Y. Ohshiro, T. Inoue, Y. Kai, N. Kasai, J. Am. Chem. Soc. 115 (1993) 9960.
[16] S. Itoh, H. Kawakami, S. Fukuzumi, Biochemistry 37 (1998) 6562.
[17] Z. Xia, Y. He, W. Dai, S.A. White, G.D. Boyd, F.S. Mathews, Biochemistry 38 (1999) 1214.

[18] Z. Xia, W. Dai, Y. Zhang, S.A. White, G.D. Boyd, F.S. Mathews, J. Mol. Biol. 259 (1996) 480.
[19] M. Ghosh, C. Anthony, K. Harlos, M.G. Goodwin, C. Blake, Structure 3 (1995) 177.
[20] M.J. Frisch, G.W. Trucks, H.B. Schlegel, G.E. Scuseria, M.A. Robb, J.R. Cheeseman, V.G. Zakrzewski, J.J.A. Montgomery, R.E. Stratmann, J.C. Burant, S. Dapprich, J.M. Millam, A.D. Daniels, K.N. Kudin, M.C. Strain, O. Farkas, J. Tomasi, V. Barone, M. Cossi, R. Cammi, B. Mennucci, C. Pomelli, C. Adamo, S. Clifford, J. Ochterski, G.A. Petersson, P.Y. Ayala, Q. Cui, K. Morokuma, D.K. Malick, A.D. Rabuck, K. Raghavachari, J.B. Foresman, J. Cioslowski, J.V. Ortiz, B.B. Stefanov, G. Liu, A. Liashenko, P. Piskorz, I. Komaromi, R. Gomperts, R.L. Martin, D.J. Fox, T. Keith, M.A. Al-Laham, C.Y. Peng, A. Nanayakkara, C. Gonzalez, M. Challacombe, P.M.W. Gill, B. Johnson, W. Chen, M.W. Wong, J.L. Andres, C. Gonzalez, M. Head-Gordon, E.S. Replogle, J.A. Pople, GAUSSIAN 98, Gaussian Inc., Pittsburgh, PA, 1998.
[21] B.H. Besler, K.M. Merz, P.A. Kollman, J. Comput. Chem. 11 (1990) 431.
[22] C.I. Bayly, P. Cieplak, W.D. Cornell, P.A. Kollman, J. Phys. Chem. 97 (1993) 10269.
[23] B.R. Brooks, R.E. Bruccoleri, B.D. Olason, D.J. States, S. Swaminathan, M. Karplus, J. Comput. Chem. 4 (1983) 187.
[24] A.D. MacKerell, D. Bashford, M. Bellott, J.R.L. Dunbrack, J.D. Evanseck, M.J. Field, S. Fischer, J. Gao, H. Guo, S. Ha, D. Joseph-McCarthy, L. Kuchnir, K. Kuczera, F.T.K. Lau, C. Mattos, S. Michnick, T. Ngo, D.T. Nguyen, B. Prodhom, W.E.I. Reiher, B. Roux, M. Schlenkrich, J.C. Smith, R. Stote, J. Straub, M. Watanabe, J. Wiorkiewicz-Kuczera, D. Yin, M. Karplus, J. Phys. Chem. B 102 (1998) 3586.
[25] W. Jorgensen, J. Chandrasekhar, J. Madhura, R. Impey, M. Klein, J. Chem. Phys. 79 (1983) 926.
[26] C.L. Brooks, M. Karplus, J. Mol. Biol. 208 (1989) 159.
[27] J.P. Ryckaert, G. Ciccotti, H.J.C. Berendsen, J. Comput. Phys. 23 (1977) 327.
[28] A. Avezoux, M. Goodwin, C. Anthony, Biochem. J. 307 (1995) 735.
[29] J. Ma, X. Zheng, G. Schnappauf, G. Braus, M. Karplus, W.N. Lipscomb, Proc. Natl Acad. Sci. USA 95 (1998) 14640.